Mathematical model to study
The spread of spilled oil in the soil

Nirmala P. Ratchagar and S.V. Hemalatha

Department of Mathematics
Annamalai University
Annamalainagar - 608 002, India
nirmalapasala@yahoo.co.in, hemaazhagu@yahoo.com

Abstract

A mathematical model describing the spread of spilled oil through the soil is discussed. The spread of spilled oil in soil is controlled by the flow of water and is described by multiphase equations. In this context, the two-phase flow characteristics of oil-water flow with varying viscosity in the subsurface coupled to an advective-diffusion equation are examined to study the transport of oil. The terms that model the interaction between the multiple phases are introduced at the boundary, such as the slip condition at the porous-fluid interface, shear stress condition at the fluid-fluid interface, and the continuity of velocity at both the interfaces. The effect of various physical parameters such as Schmidt number, retardation factor, viscosity ratio, porous and slip parameter on the velocity and concentration profiles are discussed in detail with the help of graphs. The surface plots of velocity and concentration of oil against axial distance at different time are also analyzed. The obtained results show that the velocity of oil accelerates linearly with axial length and there is a decrease in the concentration of the spilled oil through the media. The validity of the results obtained is verified by comparison with available experimental result, and good agreement is found.

1.   Introduction

Oil became a source of power for transport due to the development in technology. Accidents involving spillages of oil onto the ground surface have the potential to create serious problems in terms of both soil and groundwater contamination. The identification processes of migration and degradation of oil products in soil is of great importance as it poses a health risk to humans, plants and animal lives. Most oils act as non-aqueous phase liquids (NAPLs) and their migration in the subsurface has been the focus of numerous studies.

The complex oil spill phenomena consists of three phase fluid system with air, oil and water existing in the soil. The three-phase system may be evaluated as a combination of two phase systems consisting of air/oil, air/water and oil/water. Many combinations govern the behavior of these systems in the soil. Some of them in the literature include, numerical model of multiphase immiscible flow for evaluating non-aqueous phase liquids (NAPL) such as petroleum hydrocarbons and water phase flow in a two phase (water, NAPL) and three phase (air, water and NAPL) system (Faust, 1985; Faust et al., 1989; Osborne and Sykes, 1986; Kuppusamy et al., 1987; Kaluarachchi and Parker, 1989; Panday et al., 1994). Li and Zienkiewicz (1990) and Rahman and Lewis (1999) extended the above study for deforming soil. Sabbah et al. (2004) studied the transport of polycyclic aromatic hydrocarbons in porous medium in the presence of dissolved organic matter and predicted the sorption constants of polycyclic aromatic hydrocarbons to soil and their binding constants to dissolved organic matter using breakthrough curves. Mukherjee and Shome (2009) presented an analytical solution of fingering phenomenon arising in double phase flow of water injected with constant velocity into a dipping oil saturated porous medium using calculus of variation and similarity theory.

The multiphase equation of fluid movement describes how quickly the infiltration would occur. A multiphase fluid flow equation is needed to calculate infiltration rate based on Darcy's law combined with the fluid constitutive theory, which is made from the permeability functions and retention relations. The flow of each phase obeys Darcy's law which states that the flow is linearly proportional to the pressure gradient.

The objective of the present study is to achieve fundamental understanding of the two-phase flow system in the subsurface that describe the transport of oil components dissolved in the water that occupies the void space or part of it. In an oil spill two different types of flows occur. One is the flow in the vertical direction down to the water table, under the influence of gravity; the other is the lateral spreading which occurs on the subsurface/on top of the water table. In this paper, we assume that the oil spill flows on a flat surface in a horizontal direction. Hochmuth and Sunada (1985) explained that the Dupuit-Forchheimer approximation holds this by assuming that the flow is strictly horizontal and is valid where vertical head gradients and components of flow are small relative to the horizontal (i.e. gradual water-table slopes). We restrict ourself to two-dimensional models of oil filtration in soil, which show quite well all main properties of three-dimensional models. This paper introduces a number of useful equations to study the spread of oil in soil.

2. Problem Formulation

A spill will spread to a different context if the surface is either smooth or rough with many surface depressions. Generally in nature soils seldom have a flat surface and almost always they have surfaces with complex configuration. In urban conditions there are many cases where spilled oil covers the flat surface as positive pit rectangular type. Hence, we use a rectangular coordinate system (x, y) to model this flow, where, x and y denote the horizontal and vertical coordinates, respectively. The geometry under consideration consists of three-layer regions: region I $(h_2 \leq y \leq H)$ and II $(h_1 \leq y \leq h_2)$ are assumed to be fluid regions containing oil and water, with densities ρ_1 and ρ_2, viscosities μ_1 and μ_2, respectively and region III $(0 \leq y \leq h_1)$ is the subsurface considered to be a fluid saturated porous medium initially filled with water as shown in Figure 1. For each layer, conservation of mass and momentum equations with appropriate boundary conditions at the domain boundary and interface are considered. The subsurface soil is considered to be a homogeneous porous medium bounded by fluid layers and the fluids are supposed to be incompressible and the flow is transient. These flows are modeled via solution of the Navier-Stokes equations coupled to a advective-diffusion equation for the concentration of the more viscous fluid (i.e. oil). Through an imposed pressure-gradient, the initially filled water is displaced by oil. The viscosity is modeled as an exponential function of the concentration of oil, while the density contrast is neglected. Under these assumptions, the governing equations are rendered as follows:
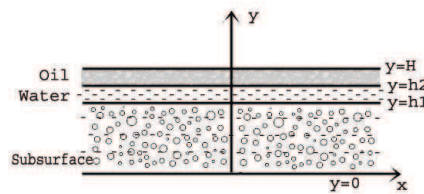

Figure 1: Physical configuration

Region I and Region II:

$$\frac{\partial u_i}{\partial x} + \frac{\partial v_i}{\partial y} = 0, \tag{1}$$

$$\frac{\partial u_i}{\partial t} + u_i \frac{\partial u_i}{\partial x} + v_i \frac{\partial u_i}{\partial y} = -\frac{1}{\rho_i} \frac{\partial p_i}{\partial x} + \nu_i \left(\frac{\partial^2 u_i}{\partial x^2} + \frac{\partial^2 u_i}{\partial y^2} \right), \tag{2}$$

$$\frac{\partial v_i}{\partial t} + u_i \frac{\partial v_i}{\partial x} + v_i \frac{\partial v_i}{\partial y} = -\frac{1}{\rho_i} \frac{\partial p_i}{\partial y} + \nu_i \left(\frac{\partial^2 v_i}{\partial x^2} + \frac{\partial^2 v_i}{\partial y^2} \right), \tag{3}$$

where, $i = 1, 2$.

Region III:

$$\frac{\partial u_3}{\partial x} + \frac{\partial v_3}{\partial y} = 0, \tag{4}$$

$$\frac{\partial u_3}{\partial t} + u_3 \frac{\partial u_3}{\partial x} + v_3 \frac{\partial u_3}{\partial y} = -\frac{1}{\rho}\frac{\partial p_3}{\partial x} + \frac{1}{\rho}\left(\frac{\partial}{\partial x}\left(\mu\frac{\partial u_3}{\partial x}\right) + \frac{\partial}{\partial y}\left(\mu\frac{\partial u_3}{\partial y}\right)\right) - \frac{1}{\rho k_p}\left(\mu u_3\right), \qquad (5)$$

$$\frac{\partial v_3}{\partial t} + u_3 \frac{\partial v_3}{\partial x} + v_3 \frac{\partial v_3}{\partial y} = -\frac{1}{\rho}\frac{\partial p_3}{\partial y} + \frac{1}{\rho}\left(\frac{\partial}{\partial x}\left(\mu\frac{\partial v_3}{\partial x}\right) + \frac{\partial}{\partial y}\left(\mu\frac{\partial v_3}{\partial y}\right)\right) - \frac{1}{\rho k_p}\left(\mu v_3\right), \qquad (6)$$

$$\rho_b \frac{\partial s}{\partial t} + \beta_w \frac{\partial c}{\partial t} + \beta_w u_3 \frac{\partial c}{\partial x} + \beta_w v_3 \frac{\partial c}{\partial y} = \beta_w D\left(\frac{\partial^2 c}{\partial x^2} + \frac{\partial^2 c}{\partial y^2}\right), \qquad (7)$$

where, u_1 and v_1 are the velocities of oil in region I, u_2 and v_2 are the velocities of oil in region II, u_3 and v_3 are the velocities of oil in region III along the x and y directions, respectively, t is the time, c is the concentration of oil in water, s is the concentration of adsorbed oil in soil, p_i represents the pressure on the regions I, II and III for $i = 1, 2, 3$, respectively, ρ_i represents the density on the regions I and II for $i = 1, 2$, respectively, ρ_b is the soil bulk density, β_w is the volumetric water content of soil, D is the mass diffusivity and k_p is the permeability of the medium. Here, the density (ρ) and viscosity (μ) of region III are scaled on that of less viscous fluid (i.e., water).

Accounting for equilibrium in linear sorption process, the retardation factor $R = 1 + \dfrac{\rho_b k_d}{\beta_w}$, where, $s = k_d C$, k_d is the adsorption coefficient, reduces equation (7) to

$$R\frac{\partial c}{\partial t} + u_3 \frac{\partial c}{\partial x} + v_3 \frac{\partial c}{\partial y} = D\left(\frac{\partial^2 c}{\partial x^2} + \frac{\partial^2 c}{\partial y^2}\right). \qquad (8)$$

The solution to the governing equations also require specification of boundary conditions. The boundary effects are modeled using Beavers-Joseph slip condition (Beavers and Joseph, 1967) at the soil-water interface $(y = h_1)$, shear stress condition at the oil-water interface $(y = h_2)$ and the continuity of velocity at both the interfaces. Under these assumptions and appropriate boundary conditions at the domain boundary, the velocity and concentration fields are defined at the boundary as

$$u_1 = v_0(1 + \epsilon e^{\mathbf{i}(\alpha x + \omega t)}), \ v_1 = 0 \ \text{ at } y = H, \qquad (9)$$

$$u_1 = u_2 \ , v_1 = v_2 \ , \frac{\partial p_1}{\partial x} = \frac{\partial p_2}{\partial x} \ , \mu_1\left(\frac{\partial u_1}{\partial y} + \frac{\partial v_1}{\partial x}\right) = \mu_2\left(\frac{\partial u_2}{\partial y} + \frac{\partial v_2}{\partial x}\right) \ \text{ at } y = h_2, \qquad (10)$$

$$\frac{\partial u_3}{\partial y} = \frac{\alpha_p}{\sqrt{k_p}}(u_3 - u_2) \ , \ \frac{\partial u_3}{\partial y} = \frac{\partial u_2}{\partial y} \ , \frac{\partial p_2}{\partial x} = \frac{\partial p_3}{\partial x} \ , \ v_2 = v_3 \ , \ c = c_0(1 + \epsilon e^{\mathbf{i}(\alpha x + \omega t)}) \ \text{ at } y = h_1,$$
$$\qquad (11)$$

$$\frac{\partial u_3}{\partial y} = -\frac{\alpha_p}{\sqrt{k_p}}(u_3 - u_2) \ , \ v_3 = v_0 \epsilon e^{\mathbf{i}(\alpha x + \omega t)} \ , \ c = c_0 \epsilon e^{\mathbf{i}(\alpha x + \omega t)} \ \text{ at } y = 0, \qquad (12)$$

where α_p is the slip parameter, α is the stream-wise wave number, ω is the frequency parameter, ϵ is the perturbation parameter, and $\mathbf{i}$ represents the imaginary part.

We now introduce the following non-dimensional quantities:

$$(x^*, y^*) = \frac{1}{H}(x, y), \quad t^* = \frac{tv_0}{H}, \quad (u_i^*, v_i^*) = \frac{1}{v_0}(u_i, v_i), \quad p_i^* = \frac{p_i}{\rho_i v_0^2}, \quad \mu^* = \frac{\mu}{\mu_2},$$

$$h_1^* = \frac{h_1}{H}, \quad h_2^* = \frac{h_2}{H}, \quad c^* = \frac{c}{c_0} \quad (i = 1, 2, 3),$$

where H, v_0, and c_0 are the characteristic height, velocity, and concentration respectively.

Making use of the non-dimensional variables in equations (1) to (6) and (8), neglecting the '*' symbol gives the following.

Region I and Region II:

$$\frac{\partial u_i}{\partial x} + \frac{\partial v_i}{\partial y} = 0, \tag{13}$$

$$\frac{\partial u_i}{\partial t} + u_i \frac{\partial u_i}{\partial x} + v_i \frac{\partial u_i}{\partial y} = -\frac{\partial p_i}{\partial x} + \frac{1}{Re_i}\left(\frac{\partial^2 u_i}{\partial x^2} + \frac{\partial^2 u_i}{\partial y^2}\right), \tag{14}$$

$$\frac{\partial v_i}{\partial t} + u_i \frac{\partial v_i}{\partial x} + v_i \frac{\partial v_i}{\partial y} = -\frac{\partial p_i}{\partial y} + \frac{1}{Re_i}\left(\frac{\partial^2 v_i}{\partial x^2} + \frac{\partial^2 v_i}{\partial y^2}\right), \tag{15}$$

where $i = 1, 2$.

Region III:

$$\frac{\partial u_3}{\partial x} + \frac{\partial v_3}{\partial y} = 0, \tag{16}$$

$$\frac{\partial u_3}{\partial t} + u_3 \frac{\partial u_3}{\partial x} + v_3 \frac{\partial u_3}{\partial y} = -\frac{\partial p_3}{\partial x} + \frac{1}{Re_3}\left(\frac{\partial}{\partial x}\left(\mu \frac{\partial u_3}{\partial x}\right) + \frac{\partial}{\partial y}\left(\mu \frac{\partial u_3}{\partial y}\right)\right) - \frac{\sigma^2}{Re_3}(\mu u_3), \tag{17}$$

$$\frac{\partial v_3}{\partial t} + u_3 \frac{\partial v_3}{\partial x} + v_3 \frac{\partial v_3}{\partial y} = -\frac{\partial p_3}{\partial y} + \frac{1}{Re_3}\left(\frac{\partial}{\partial x}\left(\mu \frac{\partial v_3}{\partial x}\right) + \frac{\partial}{\partial y}\left(\mu \frac{\partial v_3}{\partial y}\right)\right) - \frac{\sigma^2}{Re_3}(\mu v_3), \tag{18}$$

$$R\frac{\partial c}{\partial t} + u_3 \frac{\partial c}{\partial x} + v_3 \frac{\partial c}{\partial y} = \frac{1}{Re_3 Sc}\left(\frac{\partial^2 c}{\partial x^2} + \frac{\partial^2 c}{\partial y^2}\right), \tag{19}$$

where $Re_i = \frac{\rho_i v_0 H}{\mu_i}$ represents the Reynolds number on the Regions I, II and III for $i = 1, 2, 3$, respectively, $Sc = \frac{\mu_2}{\rho_2 D}$ is the Schmidt number and $\sigma = \frac{H}{\sqrt{k_p}}$ is the porous parameter.

Accordingly the non-dimensional boundary conditions are:

$$u_1 = 1 + \epsilon e^{\mathbf{i}(\alpha x + \omega t)}, \quad v_1 = 0 \quad at \ y = 1, \tag{20}$$

$$u_1 = u_2, v_1 = v_2, \frac{\partial p_1}{\partial x} = \frac{\partial p_2}{\partial x}, \mu_1\left(\frac{\partial u_1}{\partial y} + \frac{\partial v_1}{\partial x}\right) = \mu_2\left(\frac{\partial u_2}{\partial y} + \frac{\partial v_2}{\partial x}\right) \quad at \ y = h_2, \tag{21}$$

$$\frac{\partial u_3}{\partial y} = \alpha_p \sigma (u_3 - u_2) \ , \ \ \frac{\partial u_3}{\partial y} = \frac{\partial u_2}{\partial y} \ , \frac{\partial p_2}{\partial x} = \frac{\partial p_3}{\partial x} \ , \ \ v_2 = v_3 \ , \ \ c = 1 + \epsilon e^{\mathbf{i}(\alpha x + \omega t)} \ at \ y = h_1,$$

$$(22)$$

$$\frac{\partial u_3}{\partial y} = -\alpha_p \sigma (u_3 - u_2) \ , \ \ v_3 = \epsilon e^{\mathbf{i}(\alpha x + \omega t)} \ , \ \ c = \epsilon e^{\mathbf{i}(\alpha x + \omega t)} \ at \ y = 0. \tag{23}$$

3.   Method of Solution

We decompose the flow and the concentration variables into steady base state quantities (designated by upper-case letters) and two-dimensional linear perturbations (designated by a hat) as

$$(u_i, v_i, p_i, c, \mu) = (U_{B_i}(y), 0, P_{B_i}(x), C_B(y), \mu_B(y)) + (\hat{u}_i, \hat{v}_i, \hat{p}_i, \hat{c}, \hat{\mu})(y) \ \epsilon \ e^{\mathbf{i}(\alpha x + \omega t)} + o(\epsilon^2), \tag{24}$$

for $i = 1, 2, 3$. In equation (24), the base state viscosity is given by $\mu_B = e^{c_B \ ln \ m}$, where, $m = \frac{\mu_1}{\mu_2}$ is the viscosity ratio and the perturbed part viscosity is neglected for the sake of brevity. Substituting (24) into equations (13) to (19), neglecting the higher order of (ϵ^2) and equating the zeroth and first order terms, we obtain the following set of ordinary differential equations.

Base State:

By assuming a steady, parallel, fully developed flow, the base state equations obtained are:

$$\frac{d^2 U_{B_i}}{dy^2} = g_i, \quad i = 1, 2. \tag{25}$$

$$\frac{d}{dy} \left(\mu_B \frac{dU_{B_3}}{dy} \right) - \sigma^2 \mu_B U_{B_3} = g_3, \tag{26}$$

$$\frac{d^2 C_B}{dy^2} = 0, \tag{27}$$

where $g_i = Re_i \frac{dP_{B_i}}{dx}$ $(i = 1, 2, 3)$, subject to the boundary conditions,

$$U_{B_1} = 1 \ at \ y = 1 \ , \tag{28}$$

$$U_{B_1} = U_{B_2} \ , \ \ \frac{dP_{B_1}}{dx} = \frac{dP_{B_2}}{dx} \ , \ \ m \frac{dU_{B_1}}{dy} = \frac{dU_{B_2}}{dy} \ at \ y = h_2 \ , \tag{29}$$

$$\frac{dU_{B_3}}{dy} = \alpha_p \ \sigma \ (U_{B_3} - U_{B_2}) \ , \ \ \frac{dP_{B_2}}{dx} = \frac{dP_{B_3}}{dx} \ , \ \ \frac{dU_{B_3}}{dy} = \frac{dU_{B_2}}{dy} \ , \ \ C_B = 1 \ at \ y = h_1 \ , \tag{30}$$

$$\frac{dU_{B_3}}{dy} = -\alpha_p \ \sigma \ (U_{B_3} - U_{B_2}) \ , \ \ C_B = 0 \ at \ y = 0 \ . \tag{31}$$

The solution of the above equations yielding the base state velocities and concentration are

$$U_{B_1} = \frac{g_1}{2} y^2 + g_4 y + g_5, \tag{32}$$

$$U_{B_2} = \frac{g_2}{2} y^2 + g_6 y + g_7, \tag{33}$$

$$U_{B_3} = g_{11}e^{g_9 y} + g_{12}e^{g_{10} y} + g_{13}m^{-\frac{y}{h_1}}, \tag{34}$$

$$C_B = \frac{y}{h_1}. \tag{35}$$

The required constants g_i ($i = 4$ to 13) and related constants g_i ($i = 14$ to 19) and f_i ($i = 1$ to 9) are defined in the Appendix. Assuming uniform pressure ($p_1 = p_2 = p_3$) in all the three regions, the dimensionless pressure gradient is determined satisfying the condition $\int_0^{h_1} U_{B_3} dy + \int_{h_1}^{h_2} U_{B_2} dy + \int_{h_2}^1 U_{B_1} dy = 1$.

Perturbed Part:

Restricting our attention to the real parts of the solutions for the perturbed quantities, re-expressing them in terms of the stream-function $(\hat{u}_i, \hat{v}_i) = (\hat{\phi}_{iy}, -\hat{\phi}_{ix})$ for $i = 1, 2, 3$ and eliminating the pressure perturbations yields the following set of equations (after suppressing hat ($\hat{}$) symbols):

$$\phi_i^{''v} + \left[Re_i \tan(\alpha x + \omega t)\left[\omega + \alpha U_{B_i}\right] - \alpha^2 + \alpha^2 \tan^2(\alpha x + \omega t)\right]\phi_i^{''}$$
$$+ \left[Re_i \alpha^2 \tan^3(\alpha x + \omega t)\left[\omega + \alpha U_{B_i}\right] - Re_i \alpha \tan(\alpha x + \omega t)U_{B_i}'' - \alpha^4 \tan^2(\alpha x + \omega t)\right]\phi_i = 0, \tag{36}$$

for $i = 1, 2$.

$$\phi_3^{''v} + 2\mu_B' \phi_3^{'''} + \left[\mu_B'' + Re_3 \tan(\alpha x + \omega t)\left[\omega + \alpha U_{B_3}\right] + \mu_B \alpha^2 \tan^2(\alpha x + \omega t) - \mu_B \alpha^2 - \mu_B \sigma^2\right]\phi_3^{''}$$
$$+ \left[\alpha^2 \tan^2(\alpha x + \omega t) - \alpha^2 - \sigma^2\right]\mu_B' \phi_3' + \left[Re_3 \alpha^2 \tan^3(\alpha x + \omega t)\left[\omega + \alpha U_{B_3}\right]\right.$$
$$\left. - Re_3 \alpha \tan(\alpha x + \omega t)U_{B_3}'' - \alpha^2 \tan^2(\alpha x + \omega t)\left[\alpha^2 + \sigma^2\right]\mu_B\right]\phi_3 = 0, \tag{37}$$

$$c'' + \left[Re_3 Sc \tan(\alpha x + \omega t)\left[\omega R + \alpha U_{B_3}\right] - \alpha^2\right]c = Re_3 Sc \alpha \tan(\alpha x + \omega t)C_B' \phi_3, \tag{38}$$

where the prime ($'$) denotes differentiation with respect to y.

The above equations (36) to (38) are solved numerically subject to the boundary conditions outlined below.

$$\phi_1' = 1, \ \phi_1 = 0 \text{ at } y = 1, \tag{39}$$

$$\phi_1' = \phi_2', \ \phi_1 = \phi_2, \ m(\phi_1'' - \alpha^2 \tan^2(\alpha x + \omega t)\phi_1) = \phi_2'' - \alpha^2 \tan^2(\alpha x + \omega t)\phi_2,$$
$$Re_2 \left[\phi_1''' + \left[Re_1 \tan(\alpha x + \omega t)\left[\omega + \alpha U_{B_1}\right] - \alpha^2\right]\phi_1' - Re_1 \alpha \tan(\alpha x + \omega t)U_{B_1}' \phi_1\right]$$
$$= Re_1 \left[\phi_2''' + \left[Re_2 \tan(\alpha x + \omega t)\left[\omega + \alpha U_{B_2}\right] - \alpha^2\right]\phi_2' - Re_2 \alpha \tan(\alpha x + \omega t)U_{B_2}' \phi_2\right] \text{ at } y = h_2, \tag{40}$$

$$\phi_3'' = \alpha_p \sigma(\phi_3' - \phi_2'), \ \phi_2 = \phi_3, \ \phi_3'' = \phi_2'',$$
$$Re_3 \left[\phi_2''' + \left[Re_2 \tan(\alpha x + \omega t)\left[\omega + \alpha U_{B_2}\right] - \alpha^2\right]\phi_2' - Re_2 \alpha \tan(\alpha x + \omega t)U_{B_2}' \phi_2\right]$$
$$= Re_2 \left[\mu_B \phi_3''' + \mu_B' \phi_3'' + \left[Re_3 \tan(\alpha x + \omega t)\left[\omega + \alpha U_{B_3}\right] - \mu_B(\alpha^2 + \sigma^2)\right]\phi_3'\right.$$
$$\left. - Re_3 \alpha \tan(\alpha x + \omega t)U_{B_3}' \phi_3\right], \ c = 1 \text{ at } y = h_1, \tag{41}$$

$$\phi_3'' = -\alpha_p \sigma(\phi_3' - \phi_2'), \ \phi_3 = 1, \ c = 1 \ at \ y = 0 \ . \tag{42}$$

4.   Results and Discussion

We have performed computations for various pertinent parameters to understand the nature of spread of oil and its characteristics in the two-phase flow. Some of the qualitative interesting features are presented graphically.
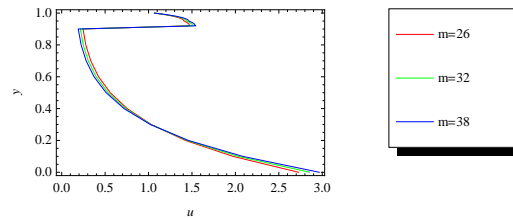

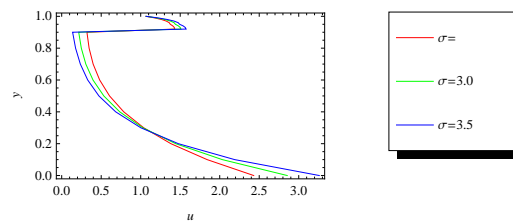
Figure 2: Effect of viscosity ratio on axial velocity
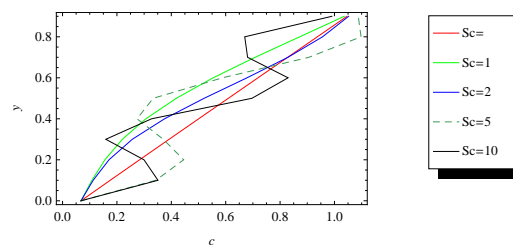

Figure 3: Effect of porous parameter on axial velocity

Figure 4: Effect of Schmidt number on concentration distribution

The axial velocity profiles for different viscosity ratio and porous parameter values are exhibited in Figures 2 and 3. The concentration distributions are described in Figures 4 to 8 for different Schmidt number, retardation factor, viscosity ratio, porous and slip parameter values. The surface plots for both the velocity and concentration are pictured in Figures 9 and 10.

The velocity of oil for different viscosity ratios is displayed in Figure 2. The effect of viscosity ratio enhances the velocity in region I and II. It is observed that the viscosity ratio is more significant in the region III. Here we see that the viscosity ratio enhances the velocity in the lower subsurface and suppresses the velocity in the upper subsurface. Physically as the viscosity ratio increases the fluid becomes more viscous reducing the velocity in the upper subsurface.
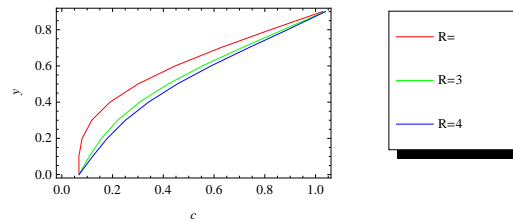
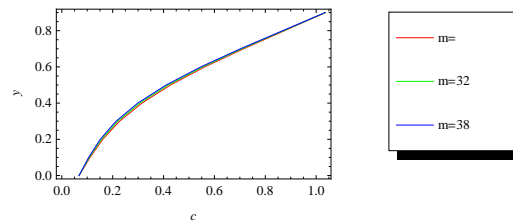Figure 5: Effect of retardation factor on concentration distribution

Figure 6: Effect of viscosity ratio on concentration distribution

Figure 3 show the velocity of oil for different porous parameter. It is seen that the effect of porous parameter are similar to that of the viscosity ratio. The discontinuity in the slope of the axial velocity at the fluid-porous interface is due to the slip effect. In the upper subsurface, the velocity decreases for increasing porous parameter indicating the fact that the effect of porosity is to retard the flow. This is due to the frictional drag resistance against the flow that decelerates the fluid flow in the porous region. As the permeability is inversely proportional to porous parameter, increase in porous parameter is due to decrease in permeability. The result agrees with the statement of Johnson et al. (1989) which states that the contaminants (the term "contaminants" is used broadly including NAPL in their study) move rapidly along the layers with higher permeability and more slowly along the lower permeability layers.

The effect of decreasing the value of Schmidt number from 10 to 0.1, thereby rendering the flow more diffusive, while keeping rest of the parameters unaltered can be seen through Figure 4. The waviness in the concentration distribution for higher Schmidt number indicates decreasing relative significance of diffusion through an increase in Schmidt number.

From Figure 5, it can be observed that the variation of the retardation factor also has a profound effect on the concentration profile as the sorption between oil components and soil surface plays an important role in the transport of oil. It can be noticed that the retardation factor R retards the oil concentration which means that at higher concentrations, retardation factor is less and at lower concentrations, retardation factor is greater.

The results of the present analysis agrees with the similar experimental results of Johnson et al. (1989) stating that the contaminant concentration arriving at a certain point at a certain time is less than it would have been for a conservative (non-retarded) contaminant. They did not consider the coupling and variable viscosity, which are included in our study.

Figure 6 describing the variation of viscosity contrast on concentration is found to be invariant.
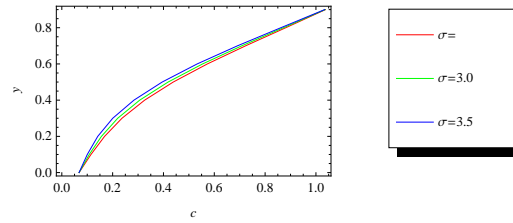
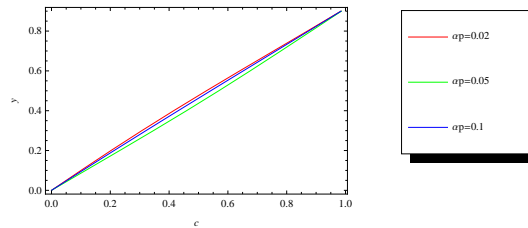Figure 7: Effect of porous parameter on concentration distribution

Figure 8: Effect of slip parameter on concentration distribution

The effect of porous parameter on the concentration profile is illustrated through Figure 7. It reveals that porous parameter enhances the concentration in the subsurface. Figure 8 representing the slip parameter effect on concentration shows that the slope of concentration remains remarkably linear, indicating approximately constant spreading.

The spatiotemporal evolution of axial velocity and concentration surface plots are depicted in Figures 9 and 10, respectively. A surface plot is used to explore the potential relationship between the predictor variables (x and t) and the response variable (axial velocity and concentration) represented by a smooth surface. Based on the regression model, the surface plot provides a clearer concept of the response surface. Figure 9 reveals that velocity of oil accelerates linearly with axial length. From the Figure 10, we come with the understanding that as the color gets darker, the response increases providing the information that there is a decrease in the concentration of the spilled oil through the subsurface.

5. Conclusion

In the present study the movement of oil flow and its characteristics in the subsurface are examined through a two-phase flow. The governing non-linear equations are solved by linearization technique wherein the flow is assumed to be in two parts, i.e. a base part and a perturbed part. The exact solutions are obtained for the base part, the perturbed part is solved numerically and the results are represented graphically for various governing parameters such as Schmidt number, retardation factor, viscosity ratio, porous and slip parameter.

In general, the analysis of the obtained results showed that the flow field is significantly influenced by these parameters, in particular, the effect is more significant in the upper subsurface. This can be identified by the Figures 2 and 3 representing the velocity of oil. Here we observe that
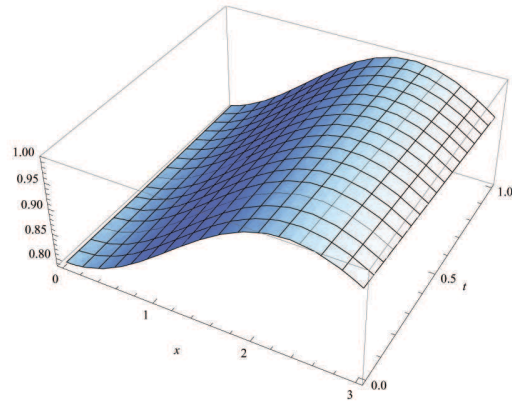
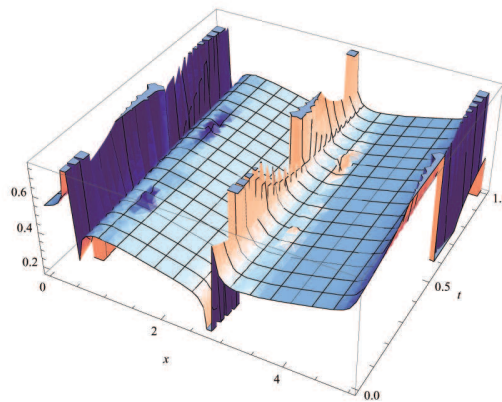Figure 9: Spatiotemporal evolution for velocity surface plot

Figure 10: Spatiotemporal evolution for concentration surface plot

the velocity of oil decreases for increase in both the viscosity ratio and porous parameter in the upper subsurface. This agrees with the result of Johnson et al. (1989) which states that the contaminants move rapidly along the layers with higher permeability and more slowly along the lower permeability layers.

The concentration of oil in the subsurface is invariant for different viscosity ratio and the porous parameter enhances the concentration. We also see that the retardation factor retards the concentration of oil. These results of the present analysis agree with the results for a one dimensional problem encountered by Johnson et al. (1989) which states that the contaminant concentration arriving at a certain point at a certain time is less than it would have been for a conservative (non-retarded) contaminant.

These investigations provide valuable information regarding the source, extent, and strength of subsurface contamination, its potential impact on groundwater, and implications for remediation. This model serves as a basis to monitor the rate of hydrocarbon contaminant in unsaturated soil, migrating through multi-flow in the soil-water environment.

REFERENCES

Beavers, G.S. and Joseph, D.D. (1967). Boundary condition at a naturally permeable wall, Journal of Fluid Mechanics, Vol. 30, pp. 197-207.

Faust, C.R. (1985). Transport of immiscible fluids within and below the unsaturated zone: A numerical model, Water Resources Research, Vol. 21, No. 4, pp. 587-596.

Faust, C.R., Guswa, J.H. and Mercer,J.W. (1989). Simulation of three-dimensional flow of immiscible fluids within and below the unsaturated zone, Water Resources Research, Vol. 25, No. 12, pp. 2449-2464.

Hochmuth, D.P. and Sunada, D.K. (1985). Ground-water model of two-phase immiscible flow in coarse material, Groundwater, Vol. 23, No. 5, pp. 617-626.

Johnson, R.L., Keely, J.F., Palmer, C.D., Suflita, J.M. and Fish, W. (1989). Transport and fate of contaminants in the subsurface, Seminar Publication, EPA/625/4-89/019.

Kaluarachchi, J.J. and Parker, J.C. (1989). An efficient finite element method for modeling multiphase flow, Water Resources Research, Vol. 25, No. 1, pp. 43-54.

Kuppusamy, T., Sheng, J., Parker, J.C. and Lenhard, R.J. (1987). Finite-element analysis of multiphase immiscible flow through soils, Water Resources Research, Vol. 23, No. 4, pp. 625-631.

Li, X.K. and Zienkiewicz, O.C. (1990). A numerical model for immiscible two-phase fluid flow in a porous medium and its time domain, International Journal for Numerical Methods in Engineering, Vol. 30, No. 6, pp. 1195-1212.

Mukherjee, B. and Shome, P. (2009). An analytic solution of fingering phenomenon arising in fluid flow through porous media by using techniques of calculus of variation and similarity theory, Journal of Mathematics Research, Vol. 1, No. 2, pp. 64-72.

Osborne, M. and Sykes, J. (1986). Numerical modeling of immiscible organic transport at the Hyde Park landfill, Water Resources Research, Vol. 22, No. 1, pp. 25-33.

Panday, S., Wu, Y.S., Huyakorn, P.S. and Springer, E.P. (1994). A three-dimensional multiphase flow model for assessing NAPL contamination in porous and fractured media, 2. Porous medium simulation examples, Journal of Contaminant Hydrology, 16, pp. 131-156.

Rahman, N.A. and Lewis, R.W. (1999). Finite element modelling of multiphase immiscible flow in deforming porous media for subsurface systems, Computers and Geotechnics, Vol. 24, No. 1, pp. 41-63.

Sabbah, I., Rebhun, M. and Gerstl, Z. (2004). An independent prediction of the effect of dissolved organic matter on the transport of polycyclic aromatic hydrocarbons, Journal of Contaminant Hydrology, Vol. 75, No. 1-2, pp. 55-70.

Appendix

$$g_4 = \frac{1}{g_{15}}\left(f_9 - (g_9 + \alpha_p\sigma)g_{11} - (g_{10} - \alpha_p\ \sigma)g_{12}\right)$$

$$g_5 = f_1 - g_4$$

$$g_6 = mg_4 - f_3$$

$$g_7 = (h_2 - 1 - h_2 m)g_4 - (f_2 - f_1 - h_2 f_3)$$

$$g_8 = \frac{\ln[m]}{h_1}$$

$$g_9 = \frac{-g_8 + \sqrt{(g_8^2 + 4\sigma^2)}}{2}$$

$$g_{10} = \frac{-g_8 - \sqrt{(g_8^2 + 4\sigma^2)}}{2}$$

$$g_{11} = \frac{1}{g_{16}}(g_{14}f_7 + mf_8 - g_{17}g_{12})$$

$$g_{12} = \frac{g_{14}g_{18}f_7 + mf_8 g_{18} - g_{15}g_{16}f_8 - g_{14}g_{16}f_9}{g_{17}g_{18} - g_{16}g_{19}}$$

$$g_{13} = \frac{g_3 h_1^2}{(\ln[m] + g_9 h_1)(\ln[m] + g_{10}h_1)}$$

$$g_{14} = -\alpha_p\sigma h_1 m + g_{15}$$

$$g_{15} = -\alpha_p\sigma(h_2 - 1 - h_2 m)$$

$$g_{16} = g_{14}g_9 e^{g_9 h_1} + m(g_9 - \alpha_p\sigma)e^{g_9 h_1}$$

$$g_{17} = g_{14}g_{10}e^{g_{10}h_1} + m(g_{10} - \alpha_p\sigma)e^{g_{10}h_1}$$

$$g_{18} = g_{15}(g_9 - \alpha_p\sigma)e^{g_9 h_1} - g_{14}(g_9 + \alpha_p\sigma)$$

$$g_{19} = g_{15}(g_{10} - \alpha_p\sigma)e^{g_{10}h_1} - g_{14}(g_{10} + \alpha_p\sigma)$$

$$f_1 = 1 - \frac{g_1}{2}$$

$$f_2 = \frac{h_2^2}{2}(g_2 - g_1)$$

$$f_3 = h_2(g_2 - mg_1)$$

$$f_4 = g_2 h_1 + \frac{g_8 g_{13}}{m}$$

$$f_5 = \frac{(g_8 + \alpha_p\sigma)g_{13}}{m} - \frac{\alpha_p\sigma g_2 h_1^2}{2}$$

$$f_6 = (g_8 - \alpha_p\sigma)g_1 3$$

$$f_7 = f_4 - f_3$$

$$f_8 = f_5 - \alpha_p\sigma h_1 f_3 - \alpha_p\sigma(f_2 - f_1 - h_2 f_3)$$

$$f_9 = f_6 - \alpha_p\sigma(f_2 - f_1 - h_2 f_3)$$